Article

SARS-CoV-2-reactive T cells in healthy donors and patients with COVID-19

https://doi.org/10.1038/s41586-020-2598-9

Received: 9 April 2020

Accepted: 22 July 2020

Published online: 29 July 2020

Check for updates

Julian Braun[1,2,17], Lucie Loyal[1,2,17], Marco Frentsch[3,4,17], Daniel Wendisch[5], Philipp Georg[5], Florian Kurth[5,6,7], Stefan Hippenstiel[5], Manuela Dingeldey[1,2], Beate Kruse[1,2], Florent Fauchere[1,2], Emre Baysal[1,2], Maike Mangold[1,2], Larissa Henze[1,2], Roland Lauster[1,8], Marcus A. Mall[4,9], Kirsten Beyer[9], Jobst Röhmel[9], Sebastian Voigt[10], Jürgen Schmitz[11], Stefan Miltenyi[11], Ilja Demuth[12], Marcel A. Müller[13], Andreas Hocke[5], Martin Witzenrath[5], Norbert Suttorp[5], Florian Kern[14,15], Ulf Reimer[15], Holger Wenschuh[15], Christian Drosten[4,13], Victor M. Corman[13], Claudia Giesecke-Thiel[16,18] ✉, Leif Erik Sander[5,18] ✉ & Andreas Thiel[1,2,18] ✉

Severe acute respiratory syndrome coronavirus 2 (SARS-CoV-2) has caused the rapidly unfolding coronavirus disease 2019 (COVID-19) pandemic[1,2]. Clinical manifestations of COVID-19 vary, ranging from asymptomatic infection to respiratory failure. The mechanisms that determine such variable outcomes remain unresolved. Here we investigated $CD4^+$ T cells that are reactive against the spike glycoprotein of SARS-CoV-2 in the peripheral blood of patients with COVID-19 and SARS-CoV-2-unexposed healthy donors. We detected spike-reactive $CD4^+$ T cells not only in 83% of patients with COVID-19 but also in 35% of healthy donors. Spike-reactive $CD4^+$ T cells in healthy donors were primarily active against C-terminal epitopes in the spike protein, which show a higher homology to spike glycoproteins of human endemic coronaviruses, compared with N-terminal epitopes. Spike-protein-reactive T cell lines generated from SARS-CoV-2-naive healthy donors responded similarly to the C-terminal region of the spike proteins of the human endemic coronaviruses 229E and OC43, as well as that of SARS-CoV-2. This results indicate that spike-protein cross-reactive T cells are present, which were probably generated during previous encounters with endemic coronaviruses. The effect of pre-existing SARS-CoV-2 cross-reactive T cells on clinical outcomes remains to be determined in larger cohorts. However, the presence of spike-protein cross-reactive T cells in a considerable fraction of the general population may affect the dynamics of the current pandemic, and has important implications for the design and analysis of upcoming trials investigating COVID-19 vaccines.

The COVID-19 pandemic poses a threat to public health and the global economy as the number of cases and COVID-19-related deaths increases worldwide[1,2]. COVID-19 is routinely diagnosed by the detection of SARS-CoV-2 RNA in nasopharyngeal swabs using PCR[3], the detection of which is reliable during the acute phase of COVID-19[4,5]. However, the limited availability of tests and the preferential testing of patients with symptoms has probably led to a marked underestimation of the infection burden and overestimation of fatality rates[6]. Serological analysis of SARS-CoV-2-induced humoral immunity could reveal asymptomatic infections, but it is not yet widely applied[7,8] and is complicated by the fact that coronavirus-induced antibody responses are variable and short-lived[9,10]. Coronavirus-induced cellular immunity is predicted to be more sustained, but remains poorly characterized. However, several T cell epitopes in the structural proteins of coronaviruses have been predicted or identified[9,11–13]. Notably, T helper (T_H) cell responses and the generation of neutralizing antibodies may be interdependent[9,14]. Studies of the SARS-CoV epidemic in 2002–2003 have shown that adaptive immune responses directed against the spike glycoprotein (S) were protective[9,15,16]. Therefore, the induction of SARS-CoV-2-specific $CD4^+$ T cells is likely to be critical in the instruction of affinity-maturated and potentially protective antibody responses[17]. We therefore examined the presence, frequencies and phenotypic characteristics of SARS-CoV-2 S-reactive T cells in patients with COVID-19 compared with SARS-CoV-2-unexposed healthy donors (HDs).

[1]Si-M/'Der Simulierte Mensch', Technische Universität Berlin and Charité–Universitätsmedizin Berlin, Berlin, Germany. [2]Regenerative Immunology and Aging, BIH Center for Regenerative Therapies, Charité–Universitätsmedizin Berlin, Berlin, Germany. [3]Department of Hematology, Oncology and Tumor Immunology, Charité–Universitätsmedizin Berlin, Berlin, Germany. [4]Berlin Institute of Health (BIH), Berlin, Germany. [5]Department of Infectious Diseases and Respiratory Medicine, Charité-Universitätsmedizin Berlin, Berlin, Germany. [6]Department of Tropical Medicine, Bernhard Nocht Institute for Tropical Medicine, University Medical Center Hamburg–Eppendorf, Hamburg, Germany. [7]I. Department of Medicine, University Medical Center Hamburg-Eppendorf, Hamburg, Germany. [8]Medical Biotechnology, Institute for Biotechnology, Technische Universität Berlin, Berlin, Germany. [9]Department of Pediatric Pulmonology, Immunology and Critical Care Medicine, Charité-Universitätsmedizin Berlin, Berlin, Germany. [10]Department of Infectious Diseases, Robert Koch Institut, Berlin, Germany. [11]Miltenyi Biotec, Bergisch Gladbach, Germany. [12]Interdisciplinary Metabolism Center, Biology of Aging (BoA) group, Charité–Universitätsmedizin Berlin, Berlin, Germany. [13]Institute of Virology, Charité–Universitätsmedizin Berlin, Berlin, Germany. [14]Department of Clinical and Experimental Medicine, Brighton and Sussex Medical School, Brighton, UK. [15]JPT Peptide Technologies, Berlin, Germany. [16]Max Planck Institute for Molecular Genetics, Berlin, Germany. [17]These authors contributed equally: Julian Braun, Lucie Loyal, Marco Frentsch. [18]These authors jointly supervised this work: Claudia Giesecke-Thiel, Leif Erik Sander, Andreas Thiel. ✉e-mail: giesecke@molgen.mpg.de; leif-erik.sander@charite.de; andreas.thiel@charite.de

Identification of S-reactive CD4$^+$ T cells

We identified S-reactive CD4$^+$ T cells by flow cytometry according to their expression of CD40L and 4-1BB after in vitro stimulation with S peptides. To this end, we designed two peptide pools (15 amino acids with 11 amino acid overlaps) that spanned the entire S protein and that contained different amounts of putative MHC-II epitopes based on epitopes identified in SARS-CoV[11–13] (Fig. 1a). SARS-CoV-2 S-peptide pool PepMix 1 (hereafter, S-I) spans the N-terminal part (amino acid residues 1–643) and includes 21 predicted SARS-CoV MHC-II epitopes (Fig. 1a, Extended Data Fig. 1 and Extended Data Table 1). The second peptide pool PepMix 2 (S-II) covered the C-terminal portion (amino acid residues 633–1273) and includes 13 predicted SARS-CoV MHC-II epitopes (Fig. 1a, Extended Data Fig. 1 and Extended Data Table 1). The peptides of the receptor-binding domain in subunit S1, which represents a major target of neutralizing antibodies, are included in S-I[18,19].

For antigen-specific stimulation, peripheral blood mononuclear cells from patients and HDs were stimulated for 16 h with S-I and S-II peptide pools (for characteristics of patients and HDs, see Table 1 and Extended Data Tables 2, 3). Antigen-reactive CD4$^+$ T cells were identified by co-expression of 4-1BB and CD40L, which enables the sensitive detection of S-reactive CD4$^+$ T cells re-activated by T cell receptor engagement ex vivo[20–22] (Fig. 2a, Extended Data Fig. 2 and Supplementary Information). In 12 (67%) and 15 (83%) out of 18 patients, we detected CD4$^+$ T cells that reacted against the S-I and S-II peptide pools, respectively (Fig. 2b, d, e). Most patients with COVID-19 with critical disease showed no reactivity to the S-I peptide pool (Extended Data Fig. 3).

Notably, S-II-reactive CD4$^+$ T cells—although at slightly lower frequencies compared with patients with COVID-19—could also be detected in 24 out of 68 HDs (35%), who are hereafter referred to as reactive healthy donors (RHDs) (Fig. 2c–e). S-I-reactive CD4$^+$ T cells could be detected in only 6 out of the 24 RHDs, that is, in 5.8% of all HDs (Fig. 2d, e). All HDs were negative for IgG antibodies that were specific to the S1 subunit, in contrast to patients with COVID-19 (Fig. 2f). We further ruled out early SARS-CoV-2 infection at initial sampling by (1) direct standard diagnosis using PCR in 10 RHDs (data not shown); (2) serological testing (Fig. 2f); and (3) by repeated serological testing at least 28 days later for 65 out of 68 HDs (Extended Data Fig. 4).

We further phenotypically and functionally characterized S-reactive CD4$^+$ T cells in additional patients with COVID-19 (Extended Data Table 4) and RHDs. Notably, in both groups, SARS-CoV-2 S-II-reactive CD4$^+$ T cells exhibited a memory phenotype and a significant proportion of the cells expressed IFNγ, indicative of T_H1 polarization (Fig. 2g and Extended Data Fig. 5a–d). Most S-reactive CD4$^+$ T cells expressed IL-2 but only few cells expressed IL-17A (Extended Data Fig. 5a–d). Frequencies of S-II-reactive CD4$^+$ T cells that expressed IFNγ were similar in patients and RHDs (Fig. 2g). Testing for TNF expression revealed that S-II-reactive IFNγ$^+$CD4$^+$ T cells from RHDs mostly co-expressed TNF, whereas S-II-reactive IFNγ$^+$CD4$^+$ T cells from patients with COVID-19 showed heterogenous TNF expression patterns (Extended Data Fig. 5e). This probably reflects the different disease stages of the acute SARS-CoV-2 infection of the individual patients included in our study. These results show that S-reactive CD4$^+$ T cells with a predominantly T_H1 memory phenotype are present not only in patients with COVID-19 but also in seronegative SARS-CoV-2-unexposed HDs.

Table 1 | Baseline characteristics of all donors

Cohort	Gender distribution (%)	Average age (range)	Disease severity	ICU (yes/no)	Average sampling day (range)
Patients with COVID-19	Male, 72%; female, 28%	52.6 years (21–81 years)	Mild, 38.9%; severe, 27.8%; critical, 33.3%	No, 44.4%; yes, 55.6%	14.9 days (2–39 days)
Healthy donors	Male, 31%; female, 59%	41.9 (20–64 years)	NA	NA	NA

'Sampling day' indicates the day of sampling in days after the onset of symptoms. ICU, intensive care unit. NA, not applicable.

S-reactive T cells in RHDs are cross-reactive to hCoVs

S-reactive CD4$^+$ T cells from patients with COVID-19 equally targeted both the N-terminal (S-I) and C-terminal peptide pools (S-II) of S, whereas S-reactive CD4$^+$ T cells from RHDs reacted significantly more strongly to the S-II peptide pool (Fig. 2d). S-II exhibits a higher homology to the human endemic coronaviruses (hCoVs; known as 'common cold' viruses) 229E, NL63, OC43 and HKU1 with regard to the SARS-CoV MHC-II epitopes, compared to the S-I peptide pool (Extended Data Table 1 and Extended Data Fig. 1). This suggests that S-reactivity in SARS-CoV-2-naive HDs originated from previous immune responses

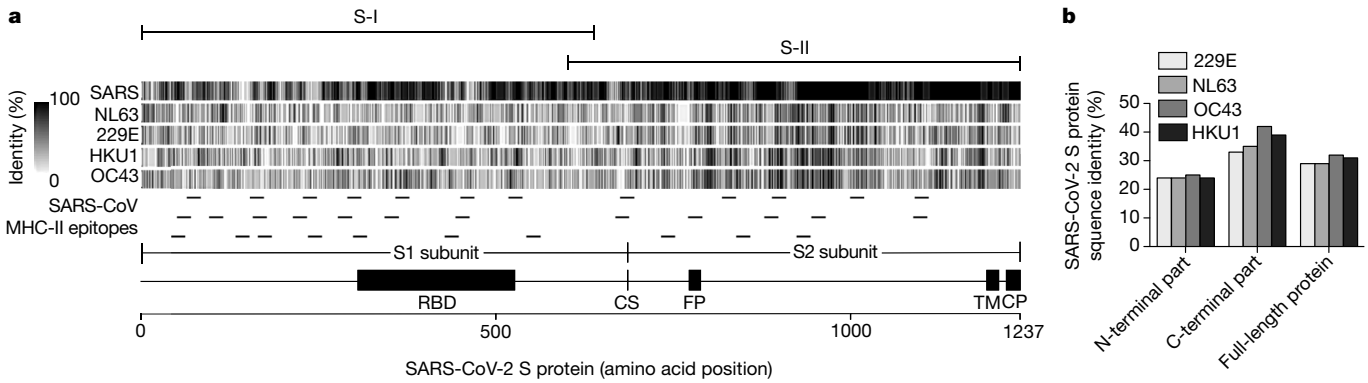

Fig. 1 | Structural domains, homology and MHC-II epitopes of the SARS-CoV-2 S protein. a, The S protein of SARS-CoV-2 (1,237 amino acids) is separated at the cleavage site (CS) into subunit S1, which comprises the receptor-binding domain (RBD), and subunit S2 which contains the fusion peptide (FP), the transmembrane domain (TM) and the cytoplasmic peptide (CP). Sequence homology of S proteins of SARS-CoV-2, SARS-CoV and hCoV strains NL63, 229E, HKU1 and OC43 was calculated as the percentage of amino acid identity in sliding windows of 10 amino acids and is depicted as grey vertical lines. Predicted SARS-CoV MHC-II epitopes are indicated as small horizontal lines. Sequences and references are listed in Extended Data Table 1. Homology is depicted for each reported MHC-II epitope in Extended Data Fig. 1. S-I spans the N-terminal region of S and S-II spans the C-terminal part of S, as indicated above the alignment. **b**, Proportion of sequence identity of the N-terminal and C-terminal parts of the S protein of SARS-CoV-2 and the S proteins of hCoV strains NL63, 229E, HKU1 and OC43.

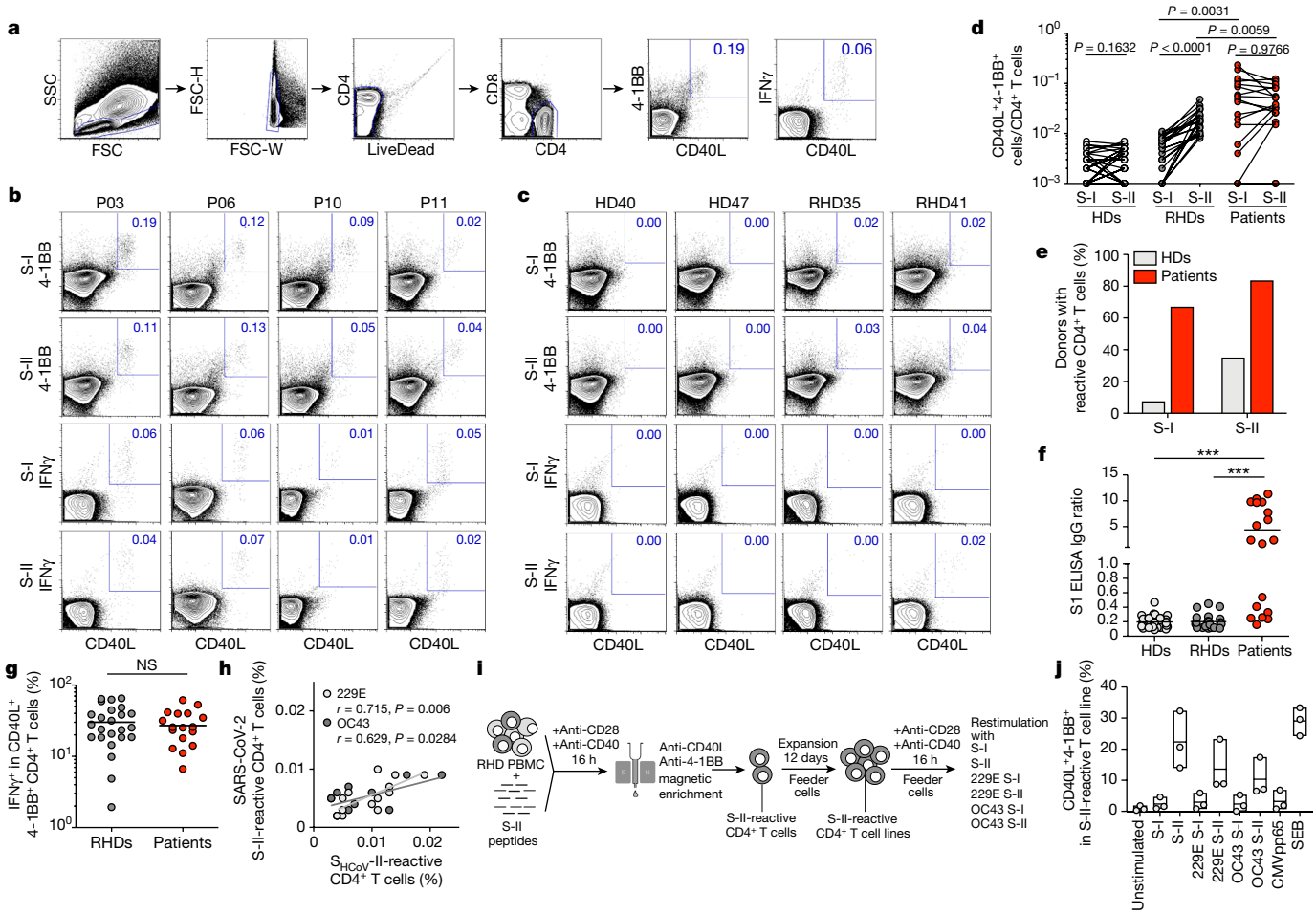

Fig. 2 | SARS-CoV-2 S-reactive CD4$^+$ T cells in patients with COVID-19 and HDs. a, Gating strategy to detect SARS-CoV-2 S-reactive CD4$^+$ T cells after in vitro stimulation for 16 h with SARS-CoV-2 S-I and S-II peptide pools. Representative data of one patient with COVID-19 are shown. FSC, forward scatter; FSC-H, forward scatter height; FSC-W, forward scatter width; SSC, side scatter. **b**, **c**, Representative plots of CD40L and 4-1BB as well as CD40L and IFNγ expression on CD4$^+$ T cells of patients with COVID-19 (P), HDs and RHDs after 16 h of in vitro stimulation with S-I or S-II peptide pools. Numbers show the percentage of double-positive cells out of the total number of CD4$^+$ T cells. **d**, Comparison of S-I- or S-II-reactive CD40L$^+$4-1BB$^+$CD4$^+$ T cell frequencies in HDs ($n = 44$), RHDs ($n = 24$) and patients ($n = 18$). **e**, Percentage of patients and HDs with S-I-reactive and S-II-reactive CD4$^+$ T cells. **f**, SARS-CoV-2 S1 serology of HDs ($n = 44$), RHDs ($n = 24$) and patients ($n = 18$). ***$P < 0.0001$. **g**, Comparison of the frequencies of IFNγ$^+$ cells among CD40L$^+$4-1BB$^+$CD4$^+$ T cells in RHDs ($n = 24$) and patients ($n = 18$). NS, not significant. **h**, Correlation between SARS-CoV-2 S-II and S_{hCoV}-II CD4$^+$ T cell responses. Frequencies of CD40L$^+$4-1BB$^+$CD4$^+$ T cells after stimulation with S-II peptide pools of SARS-CoV-2 (*y* axis) and S-II peptide pools of hCoVs (*x* axis) 229E (light grey, $n = 12$) and OC43 (dark grey, $n = 9$) from RHDs are shown. **i**, Schematic summary of the generation of SARS-CoV-2 S-II-reactive CD4$^+$ T cell lines. PBMC, peripheral blood mononuclear cells. **j**, Enriched and expanded SARS-CoV-2 S-II-reactive CD4$^+$ T cells were restimulated with the indicated S-I and S-II peptide pools of SARS-CoV-2 and the two hCoV strains. SEB, staphylococcal enterotoxin B. **d**, **f**, **g**, Significance was calculated using two-tailed Mann–Whitney *U*-tests. **h**, The correlation coefficient *r* was calculated using a bivariate Pearson correlation and the related *P* value was based on a *t*-distribution.

to hCoVs. We therefore tested 18 out of the 68 HDs for the presence of antibodies that are specific for the four endemic hCoVs. We detected IgG antibodies against all four hCoVs in all tested HDs, regardless of the presence of measurable S-reactive CD4$^+$ T cells (Extended Data Fig. 6a). Frequencies of S-reactive or -cross-reactive CD4$^+$ T cells in RHDs did not correlate with antibody levels against hCoVs, which potentially indicates that these antibodies have not been generated very recently. Similar findings have been obtained for other anti-viral CD4$^+$ T cell responses, for example, after yellow fever vaccination (YFV-17D). CD4$^+$ T cell responses showed a significant correlation with the later generation of high titres of neutralizing antibodies only at very early time points after YFV-17D vaccination[23].

We next determined whether SARS-CoV-2 S-reactive CD4$^+$ T cells in RHDs correlated with a CD4$^+$ T cell response to the S protein of endemic hCoVs (S_{hCoV}). To this end, peripheral blood mononuclear cells from HDs and RHDs were stimulated with S-I and S-II pools from SARS-CoV-2 and S_{hCoV}-I and S_{hCoV}-II pools of OC43 and 229E (Fig. 2h and Extended Data Fig. 6b–d). There was a strong positive correlation of CD4$^+$ T cell reactivity against S-II and S_{hCoV}-II of OC43 and 229E ($r = 0.629$ and $r = 0.715$, respectively) (Fig. 2h), whereas no or only a weak negative correlation was detected between S-I reactivity and reactivity towards S_{hCoV}-I of OC43 and 229E ($r = 0.037$ and $r = -0.259$, respectively) (Extended Data Fig. 6b). No correlation was observed between reactivity to S-I or S-II and CMVpp65 (Extended Data Fig. 6c, d).

We next tested whether the S-reactive CD4$^+$ T cells of RHDs responded to stimulation with S_{hCoV}. To this end, S-II-reactive CD4$^+$ T cells were isolated from three RHDs (RHD01, RHD07 and RHD15), expanded ex vivo for 12 days and subsequently restimulated with S_{hCoV}-I and S_{hCoV}-II of OC43 and 229E, with the S-II pool as positive control, or with S-I and a peptide pool from CMVpp65 as negative controls (Fig. 2i, j). Restimulation with the SARS-CoV-2 S-II peptide pool induced the highest frequencies of 4-1BB$^+$CD40L$^+$CD4$^+$ T cells, whereas negligible responses were measured in the negative controls (S-I, CMVpp65 and unstimulated groups), demonstrating the high specificity of the

established S-II-reactive CD4$^+$ T cell lines (Fig. 2j). By contrast, strong responses were observed against the S_{hCoV}-II peptide pools of the two hCoVs (Fig. 2j). These findings provide evidence of the cross-reactivity of SARS-CoV-2 S-II-reactive cells to S_{hCoV} in the tested RHDs, suggesting that pre-existence of SARS-CoV-2-reactive T cells in seronegative SARS-CoV-2-naive individuals originates from previous immune responses to endemic hCoVs.

Activation signatures in patients with COVID-19

Finally, we assessed additional activation marker profiles on S-reactive T cells from patients with COVID-19 and RHDs. Expression of CD38, HLA-DR and Ki-67 has previously been shown to reliably characterize recently in vivo activated human T cells during acute and chronic infections[24–28]. Notably, S-reactive CD4$^+$ T cells from patients largely expressed CD38, HLA-DR and Ki-67 (Fig. 3a–d). Most S-reactive T cells in patients co-expressed CD38 and HLA-DR (Fig. 3e), which is characteristic of effector T cell responses during acute viral infections[24,26], whereas CD38 and Ki-67 co-expression was more variable (Fig. 3f). By contrast, S-reactive CD4$^+$ T cells from RHDs did not express CD38, HLA-DR and Ki-67, or only at low frequencies (Fig. 3b–f), and co-expression was not observed (Fig. 3e, f). In patients, considerable proportions of the entire peripheral CD4$^+$ and CD8$^+$ T cell populations co-expressed CD38 and HLA-DR (data not shown); however, these cells could not be re-activated with our S peptide pools in vitro. These findings are consistent with results of a recent study that showed refractory T cell signatures in patients with COVID-19[29]. Additionally, a proportion of these CD38$^+$HLA-DR$^+$CD4$^+$ T cells probably targets other structural proteins of SARS-CoV-2. We furthermore show that the presence of S-reactive CD4$^+$ T cells and, in particular, of CD38-expressing cells among S-reactive CD4$^+$ T cells was highly variable among patients during the course of COVID-19 disease (Fig. 3g, h).

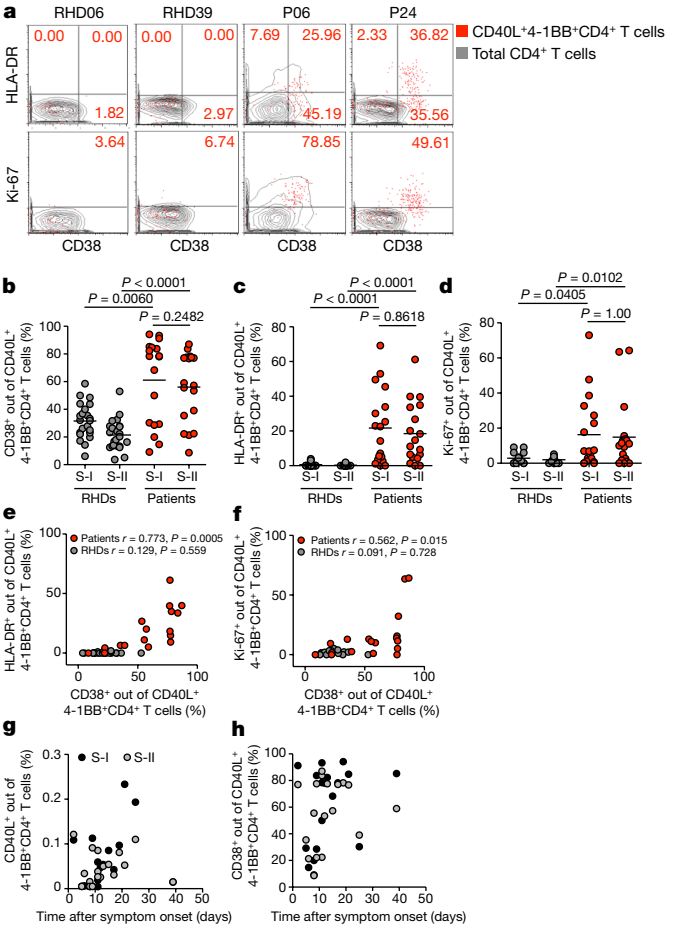

Fig. 3 | CD38, HLA-DR and Ki-67 expression in SARS-CoV-2 S-I-reactive and S-II-reactive CD4$^+$ T cells discriminates patients with COVID-19 from RHDs. **a**, Representative examples of HLA-DR and Ki-67 expression plotted against CD38 expression for S-II-reactive CD4$^+$ T cells (red dots) compared with total CD4$^+$ T cells (grey contours) in RHDs and patients with COVID-19. **b**–**d**, Comparison of frequencies of CD38$^+$, HLA-DR$^+$ and Ki-67$^+$ cells among S-I-reactive and S-II-reactive CD4$^+$ T cells in RHDs (**b**, **c**, $n = 23$; **d**, $n = 17$) and patients ($n = 18$). Significance was calculated using two-tailed Mann–Whitney *U*-tests. **e**, **f**, Co-expression of HLA-DR or Ki-67 and CD38 among S-II-reactive CD4$^+$ T cells from RHDs (**e**, $n = 23$; **f**, $n = 17$) and patients ($n = 18$). The correlation coefficient *r* was calculated using a bivariate Pearson correlation and the related *P* value was based on a *t*-distribution. **g**, **h**, Frequencies of S-I-reactive and S-II-reactive CD40L$^+$4-1BB$^+$CD4$^+$ T cells (**g**) or CD38$^+$ among S-II-reactive CD4$^+$ T cells (**h**) of patients ($n = 18$) plotted against time after symptom onset (days).

Discussion

Our study shows that S-reactive CD4$^+$ T cells are present in patients with COVID-19 and in a considerable proportion of SARS-CoV-2-unexposed HDs. In light of the recent emergence of SARS-CoV-2, our data raise the possibility that such pre-existing S-reactive T cells represent cross-reactive clones that were probably acquired during previous infections with endemic hCoVs. hCoVs account for approximately 20% of 'common cold' upper respiratory tract infections and are ubiquitous, although they display winter seasonality[30–32]. On the basis of epidemiological data, it may be extrapolated that adults contract an hCoV infection, on average, every two to three years. Protective antibodies may wane mid-term but cellular immunity could remain[10,13]. Although the overall homology of the amino acid sequences of the S protein is relatively low compared with spike glycoproteins from hCoVs, there is an overlap in MHC-II epitopes especially in the C-terminal domain of the peptide pools used here (Fig. 1a and Extended Data Fig. 1). This may explain the preferential reactivity of CD4$^+$ T cells to the C-terminal domain in one third of HDs.

The biological role of pre-existing S-cross-reactive CD4$^+$ T cells in 35% of HDs remains unclear. However, assuming that these cells have a protective role in SARS-CoV-2 infection, they may contribute to our understanding of the divergent manifestations of COVID-19, and the notable resilience of children and young adults to symptomatic SARS-CoV-2 infection. Young adults and, especially, children in day-care centres have more frequent social contacts than elderly individuals, and this may therefore lead to a higher hCoV prevalence. This hypothesis requires further investigation in future longitudinal studies that assess the presence of pre-existing SARS-CoV-2-cross-reactive CD4$^+$ T cells and their influence on the susceptibility to SARS-CoV-2 infection and age-related clinical outcomes of COVID-19.

SARS-CoV-neutralizing antibodies are associated with convalescence, and they have been detected 12 months after disease[9]. However, the durability of neutralizing antibody responses against SARS-CoV-2 remains unknown. Although antibodies against hCoV can wane within months after infection, hCoV reinfection is accompanied by low-level and short-lived virus shedding with only mild symptoms of short duration, which indicates humoral-independent residual immunity[10]. Cellular immunity has not yet been studied in this context. In mouse models, however, CD4$^+$ as well as CD8$^+$ T cell responses directed against structural proteins such as the spike or nucleocapsid proteins of SARS-CoV critically contributed to viral clearance[15,33,34]. Understanding the extent to which and how SARS-CoV-2-specific humoral or cellular immunity mediates durable protection against reinfection is of critical importance in the coming months.

Our study reveals pre-existing cellular SARS-CoV-2 cross-reactivity in a substantial proportion of SARS-CoV-2-seronegative HDs. This finding could have considerable epidemiological implications regarding

herd immunity thresholds and projections for the COVID-19 pandemic. Our results provide a decisive rationale to initiate worldwide prospective studies to assess the contribution of pre-existing, potentially region-dependent, SARS-CoV-2-cross-reactive immunity to the diverse clinical outcomes of SARS-CoV-2 infection. Together with currently introduced serological tests, the data generated by such studies may critically inform evidence-based risk evaluation, patient monitoring, adaptation of containment methods and vaccine development.

Online content

Any methods, additional references, Nature Research reporting summaries, source data, extended data, supplementary information, acknowledgements, peer review information; details of author contributions and competing interests; and statements of data and code availability are available at https://doi.org/10.1038/s41586-020-2598-9.

1. Dong, E., Du, H. & Gardner, L. An interactive web-based dashboard to track COVID-19 in real time. *Lancet Infect. Dis.* **20**, 533–534 (2020).
2. Wang, D. et al. Clinical characteristics of 138 hospitalized patients with 2019 novel coronavirus-infected pneumonia in Wuhan, China. *J. Am. Med. Assoc.* **323**, 1061–1069 (2020).
3. Corman, V. M. et al. Detection of 2019 novel coronavirus (2019-nCoV) by real-time RT-PCR. *Euro Surveill.* **25**, 2000045 (2020).
4. Loeffelholz, M. J. & Tang, Y.-W. Laboratory diagnosis of emerging human coronavirus infections — the state of the art. *Emerg. Microbes Infect.* **9**, 747–756 (2020).
5. Wölfel, R. et al. Virological assessment of hospitalized patients with COVID-2019. *Nature* **581**, 465–469 (2020).
6. Wu, J. T., Leung, K. & Leung, G. M. Nowcasting and forecasting the potential domestic and international spread of the 2019-nCoV outbreak originating in Wuhan, China: a modelling study. *Lancet* **395**, 689–697 (2020).
7. Amanat, F. et al. A serological assay to detect SARS-CoV-2 seroconversion in humans. *Nat. Med.* **26**, 1033–1036 (2020).
8. Okba, N. M. A. et al. Severe acute respiratory syndrome coronavirus 2-specific antibody responses in coronavirus disease patients. *Emerg. Infect. Dis.* **26**, 1478–1488 (2020).
9. Li, C. K. et al. T cell responses to whole SARS coronavirus in humans. *J. Immunol.* **181**, 5490–5500 (2008).
10. Callow, K. A., Parry, H. F., Sergeant, M. & Tyrrell, D. A. J. The time course of the immune response to experimental coronavirus infection of man. *Epidemiol. Infect.* **105**, 435–446 (1990).
11. Libraty, D. H., O'Neil, K. M., Baker, L. M., Acosta, L. P. & Olveda, R. M. Human CD4$^+$ memory T-lymphocyte responses to SARS coronavirus infection. *Virology* **368**, 317–321 (2007).
12. Yang, J. et al. Searching immunodominant epitopes prior to epidemic: HLA class II-restricted SARS-CoV spike protein epitopes in unexposed individuals. *Int. Immunol.* **21**, 63–71 (2009).
13. Ng, O. W. et al. Memory T cell responses targeting the SARS coronavirus persist up to 11 years post-infection. *Vaccine* **34**, 2008–2014 (2016).
14. Mitchison, N. A. T-cell–B-cell cooperation. *Nat. Rev. Immunol.* **4**, 308–312 (2004).
15. Yang, Z. Y. et al. A DNA vaccine induces SARS coronavirus neutralization and protective immunity in mice. *Nature* **428**, 561–564 (2004).
16. Zhu, Z. et al. Potent cross-reactive neutralization of SARS coronavirus isolates by human monoclonal antibodies. *Proc. Natl Acad. Sci. USA* **104**, 12123–12128 (2007).
17. Ju, B. et al. Human neutralizing antibodies elicited by SARS-CoV-2 infection. *Nature* **584**, 115–119 (2020).
18. Meng, T. et al. The insert sequence in SARS-CoV-2 enhances spike protein cleavage by TMPRSS. Preprint at https://www.biorxiv.org/content/10.1101/2020.02.08.926006v3 (2020).
19. Walls, A. C. et al. Structure, function, and antigenicity of the SARS-CoV-2 spike glycoprotein. *Cell* **181**, 281–292 (2020).
20. Frentsch, M. et al. Direct access to CD4$^+$ T cells specific for defined antigens according to CD154 expression. *Nat. Med.* **11**, 1118–1124 (2005).
21. Sattler, A. et al. Cytokine-induced human IFN-γ-secreting effector-memory Th cells in chronic autoimmune inflammation. *Blood* **113**, 1948–1956 (2009).
22. Schoenbrunn, A. et al. A converse 4-1BB and CD40 ligand expression pattern delineates activated regulatory T cells (Treg) and conventional T cells enabling direct isolation of alloantigen-reactive natural Foxp3$^+$ Treg. *J. Immunol.* **189**, 5985–5994 (2012).
23. Kohler, S. et al. The early cellular signatures of protective immunity induced by live viral vaccination. *Eur. J. Immunol.* **42**, 2363–2373 (2012).
24. Appay, V. et al. Memory CD8$^+$ T cells vary in differentiation phenotype in different persistent virus infections. *Nat. Med.* **8**, 379–385 (2002).
25. Blom, K. et al. Temporal dynamics of the primary human T cell response to yellow fever virus 17D as it matures from an effector- to a memory-type response. *J. Immunol.* **190**, 2150–2158 (2013).
26. Callan, M. F. C. et al. Direct visualization of antigen-specific CD8$^+$ T cells during the primary immune response to Epstein–Barr virus in vivo. *J. Exp. Med.* **187**, 1395–1402 (1998).
27. Miller, J. D. et al. Human effector and memory CD8$^+$ T cell responses to smallpox and yellow fever vaccines. *Immunity* **28**, 710–722 (2008).
28. Schulz, A. R. et al. Low thymic activity and dendritic cell numbers are associated with the immune response to primary viral infection in elderly humans. *J. Immunol.* **195**, 4699–4711 (2015).
29. Diao, B. et al. Reduction and functional exhaustion of T cells in patients with coronavirus disease 2019 (COVID-19). *Front. Immunol.* **11**, 827 (2020).
30. Tyrrell, D. A. J. *Common Colds and Related Diseases* (E. Arnold, 1965).
31. Lidwell, O. M. & Williams, R. E. The epidemiology of the common cold. I. *J. Hyg.* **59**, 309–319 (1961).
32. Gaunt, E. R., Hardie, A., Claas, E. C. J., Simmonds, P. & Templeton, K. E. Epidemiology and clinical presentations of the four human coronaviruses 229E, HKU1, NL63, and OC43 detected over 3 years using a novel multiplex real-time PCR method. *J. Clin. Microbiol.* **48**, 2940–2947 (2010).
33. Channappanavar, R., Fett, C., Zhao, J., Meyerholz, D. K. & Perlman, S. Virus-specific memory CD8 T cells provide substantial protection from lethal severe acute respiratory syndrome coronavirus infection. *J. Virol.* **88**, 11034–11044 (2014).
34. Wang, B. et al. Identification of an HLA-A*0201-restricted CD8$^+$ T-cell epitope SSp-1 of SARS-CoV spike protein. *Blood* **104**, 200–206 (2004).

Methods

Data reporting

No statistical methods were used to predetermine sample size. The experiments were not randomized and the investigators were not blinded to allocation during experiments and outcome assessment.

Study participants

The study was approved by the Institutional Review Board of the Charité (EA2/066/20). After providing written informed consent, 68 HDs (Table 1 and Extended Data Table 3) and 18 and 7 additional patients with COVID-19 (Table 1 and Extended Data Table 2, 4) were included in the study. Patients with COVID-19 who tested positive for SARS-CoV-2 RNA in nasopharyngeal swabs were recruited at Charité Campus Virchow-Klinikum, Berlin, between 1 March and 2 April 2020. All patients with COVID-19 were enrolled in the Berlin prospective observation COVID-19 study (PA-COVID-19)[35]. Disease severity was grouped on the basis of the requirement for supplementary oxygen or ventilation (mild, hospitalized, no supplementary oxygen; severe, hospitalized, supplementary oxygen (including high-flow oxygen); critical, hospitalized, invasive ventilation). For intracellular cytokine and memory T cell staining, seven additional patients with COVID-19 (Extended Data Table 4) were enrolled at later time points and five RHDs were re-recruited. To retrospectively validate SARS-CoV-2 seronegativity, all HDs were re-invited between 4 and 7 May 2020 for re-assessment of anti-S1 IgG titres. In total, 65 out of 68 HDs could be re-recruited and all HDs were seronegative for SARS-CoV-2 (Extended Data Fig. 4).

Serology

Anti-SARS-CoV-2 IgG ELISA was performed using a commercial kit (EUROIMMUN) as described and validated previously[8]. Recombinant immunofluorescence assays to determine IgG titres against hCoV were performed using VeroB4 cells that expressed cloned recombinant spike proteins from hCoV-229E, hCoV-NL63, hCoV-OC43 and hCoV-HKU1, as previously described[36].

Cell isolation and stimulation

Peripheral blood mononuclear cells were isolated from heparinized whole blood by density gradient centrifugation according to manufacturer's instructions (Leucosep tubes, Greiner; Biocoll, Bio&SELL). Stimulation was performed with 5×10^6 peripheral blood mononuclear cells in RPMI 1640 medium (Gibco) supplemented with 10% heat-inactivated AB serum (Pan Biotech), 100 U/ml penicillin (Biochrom), 0.1 mg/ml streptomycin (Biochrom) and PepMix SARS-CoV-2 spike glycoprotein (JPT) peptide pool 1 or 2 in the presence of 1 µg/ml purified anti-CD28 antibody (clone CD28.2, BD Biosciences). The PepMix SARS-CoV-2 spike glycoprotein pool 1 covering the N-terminal amino acid residues 1–643 (abbreviated to 'S-I' (N-term)) contained 158 15-mers that overlapped by 11 amino acids. PepMix SARS-CoV-2 spike glycoprotein pool 2 covered the C-terminal amino acid residues 633–1273 (abbreviated to 'S-II' (C-term)) contained 156 15-mers that overlapped by 11 amino acids and one 17-mer at the C terminus, that is, 157 peptides in total. Both peptide pools were used at 1 µg/ml per peptide. Further details on the peptide pools and predicted MHC-II epitopes are provided in Fig. 1, Extended Data Fig. 1 and Extended Data Table 1. Stimulation controls were performed with equal concentrations of DMSO in PBS (unstimulated) or 1.5 mg SEB/1.0 mg TSST1 (Sigma-Aldrich) and PepMix HCMVA (pp65) (>90%; CMVpp65) (JPT) in the presence of 1 µg/ml purified anti-CD28 antibody (clone CD28.2, BD Biosciences) as positive controls. Incubation was performed at 37 °C, 5% CO_2 for 16 h with 10 µg/ml brefeldin A (Sigma-Aldrich) added after 2 h. Stimulation was stopped by incubation in 2 mM EDTA for 5 min. Stimulation with hCoV spike glycoprotein (S_{hCoV}) peptide pools was performed using the conditions described above but with 1 µg/ml per peptide of the following peptide pools: PepMix hCoV-229E spike glycoprotein pool 1 or 2 or PepMix hCoV-OC43 spike glycoprotein pool 1 or 2 (all JPT).

Flow cytometry

After stimulation, staining of surface antigens was carried out for 15 min with the following fluorochrome-conjugated antibodies titrated to their optimal concentrations: CD38-PE-Vio770 (clone REA671, Miltenyi, 1:400), CD69-APC-Cy7 (FN50, BioLegend, 1:100), HLAD-DR-VioGreen (REA805, Miltenyi, 1:50), CD4-BrilliantViolet605 (RPA-T4, BioLegend, 1:200), CD8-PerCP (SK1, BioLegend, 1:100) with 1 mg/ml beriglobin (CSL Behring) added before the staining. To exclude dead cells, Zombie Yellow fixable viability staining (BioLegend) was added for the last 10 min of incubation. Fixation and permeabilization were performed with eBioscience FoxP3 fixation and PermBuffer (Invitrogen) according to the manufacturer's protocol and intracellular staining was carried out for 30 min in the dark at room temperature with beriglobin added before staining with 4-1BB-PE (4-1BB is also known as CD137; clone 4B4-1, BD, 1:10), CD40L-APC (CD40L is also known as CD154; 5C8, Miltenyi, 1:40), IFNγ-AlexaFluor700 (B27, BD, 1:50), TNF-PacificBlue (MAb11, BioLegend, 1:100) and Ki-67-AlexaFluor488 (B56, BD, 1:100). To assess naive/memory T cell phenotypes and cytokine expression, the following antibodies were used: surface staining was performed with CD3-V500 (SP34-2, BD, 1:50), CD8-PerCP (SK1, BioLegend, 1:100), CD4-BrilliantViolet605 (RPA-T4, BioLegend, 1:200), CCR7-AlexaFluor488 (G043H7, BioLegend, 1:150), CD45RA-PE-Cy7 (HI100, BioLegend, 1:200). IFNγ-AlexaFluor700 (B27, BD, 1:100), CD40L-BrilliantViolet421 (24-31, BioLegend, 1:200), IL-2-APC (5344.111, BD, 1:200), 4-1BB-PE (4B4-1, BD, 1:10) and IL-17A-APC-Cy7 (BL168, BioLegend, 1:20) were used for intracellular staining after fixation and permeabilization using BD FACSLysing Buffer and BD Perm2 Buffer, according to the manufacturer's instructions. Samples were measured on a MACSQuant Analyzer 16 using MACSQuantify software (v.2.13). Instrument performance was monitored daily with Rainbow Calibration Particles (BD).

Cell enrichment, expansion and restimulation

S-II-reactive T cells were enriched by magnetic cell sorting (MACS) from peripheral blood mononuclear cells stimulated with PepMix SARS-CoV-2 spike glycoprotein peptide pool 2 (JPT) in the presence of 1 µg/ml purified anti-CD28 (clone CD28.2, BD Biosciences) and 1 µg/ml anti-CD40 (clone 5C3, BioLegend) antibodies. After stimulation for 16 h, cells were stained with CD40L-APC and 4-1BB-PE and first enriched with anti-APC MultiSort MicroBeads (Miltenyi) according to the manufacturer's instructions. After the release of anti-APC-MicroBeads, a second enrichment was performed with anti-PE MicroBeads (Miltenyi). Purity was checked each time to >80% of alive cells. Antigen presenting feeder cells were generated by CD3 MicroBead (Miltenyi) depletion of the CD40L-APC-negative fraction and subsequent inactivation by irradiation at 50 Gy. The irradiated feeder cells were co-cultured with the enriched 4-1BB$^+$CD40L$^+$ T cells at a ratio of 1:1 in RPMI 1640 medium (Gibco) supplemented with 10% heat-inactivated AB serum (Pan Biotech), 100 U/ml penicillin (Biochrom), 0.1 mg/ml streptomycin (Biochrom) in the presence of 10 ng/ml IL-7 and IL-15 (both Miltenyi) for 12 days followed by 2-day cytokine starvation before restimulation. Restimulation was carried with the conditions described above and additionally with 1 µg/ml per peptide of the following peptide pools: PepMix hCoV-229E spike glycoprotein pool 1 or 2 or PepMix hCoV-OC43 spike glycoprotein pool 1 or 2 (all JPT).

Data analysis and statistics

Sequence alignments were performed using R (v.3.6.1) including package ClustalX[37] and using the Needlemann–Wunsch algorithm[38]. Flow cytometry data were analysed with FlowJo v.9.9.6 (FlowJo). Microsoft Excel (v.14.1.0) and Prism 5 and 8 (GraphPad) were used for plotting and statistical analysis. In stimulation experiments, frequencies of activated CD4$^+$ T cells were background-subtracted, with the frequency in the unstimulated control sample representing the background.

Non-parametric testing was used to compare cell frequencies and antibody titres between groups (two-tailed Mann–Whitney *U*-test). *n* indicates the number of donors.

Reporting summary

Further information on research design is available in the Nature Research Reporting Summary linked to this paper.

Data availability

All flow cytometry data are made available at www.FlowRepository.org (experiment ID: FR-FCM-Z2K3). The individual gating strategies for all donors are shown in Supplementary Information.

35. Kurth, F. et al. Studying the pathophysiology of coronavirus disease 2019: a protocol for the Berlin prospective COVID-19 patient cohort (Pa-COVID-19). *Infection* **48**, 619–626 (2020).
36. Corman, V. M. et al. Assays for laboratory confirmation of novel human coronavirus (hCoV-EMC) infections. *Euro Surveill.* **17**, 20334 (2012).
37. Larkin, M. A. et al. Clustal W and Clustal X version 2.0. *Bioinformatics* **23**, 2947–2948 (2007).
38. Needleman, S. B. & Wunsch, C. D. A general method applicable to the search for similarities in the amino acid sequence of two proteins. *J. Mol. Biol.* **48**, 443–453 (1970).

Acknowledgements We thank U. Klein and H.-P. Herzel for discussion; T. Kaiser and J. Kirsch from the Flow Cytometry Core Facility (FCCF) of the DRFZ for technical help; and B. Timmerman from the Sequencing Core Facility of the Max Planck Institute for Molecular Genetics for discussion. This work was supported by the German Research Foundation (KFO339 to J.B. and F.F., SFB-TR84 projects A4 and B6 to S.H., B8 to M.M., C6 to M.W., C8 and C10 to L.E.S., and C9 to M.W. and N.S.) and by the German Federal Ministry of Education and Research (BMBF-RAPID to S.H. and C.D., and CAPSyS to M.W. and N.S.). This work was additionally funded by the Federal Ministry of Health through a resolution of the German Bundestag to A.T., J.B., L.H. and M.D.

Author contributions J.B., L.L. and M.F. planned and performed experiments and analysed the data. D.W., P.G., J.R., M.D., B.K., F.F., E.B., M.M. and L.H. performed experiments. F. Kurth, A.H., S.H., K.B., I.D., M. A. Mall, S.V., M.W., N.S., C.D. and L.E.S. managed initial patient contacts, and designed and supervised clinical management and clinical data. M. A. Müller and V.M.C. planned and performed experiments and analysed the data. J.S. and S.M. established high-throughput analysis. R.L. designed experiments. F. Kern, U.R. and H.W. established new reagents. G.C.-T. and A.T. designed and supervised the study. C.G.-T., L.E.S. and A.T. wrote the manuscript.

Competing interests F. Kern, U.R. and H.W. are employed at JPT Peptide Technologies, who have provided peptide pools for this work. F. Kern also part-owns and is inventor on a patent describing the use of overlapping peptide pools for the stimulation of T cells. Until this patent expires, he will receive royalties on JPT PepMix sales. J.S. and S.M. are employed at Miltenyi Biotec, who provided reagents and devices for this study. All other authors declare no competing interests.

Additional information

Supplementary information is available for this paper at https://doi.org/10.1038/s41586-020-2598-9.

Correspondence and requests for materials should be addressed to C.G.-T., L.E.S. or A.T.

Peer review information *Nature* thanks Akiko Iwasaki and the other, anonymous, reviewer(s) for their contribution to the peer review of this work. Peer reviewer reports are available.

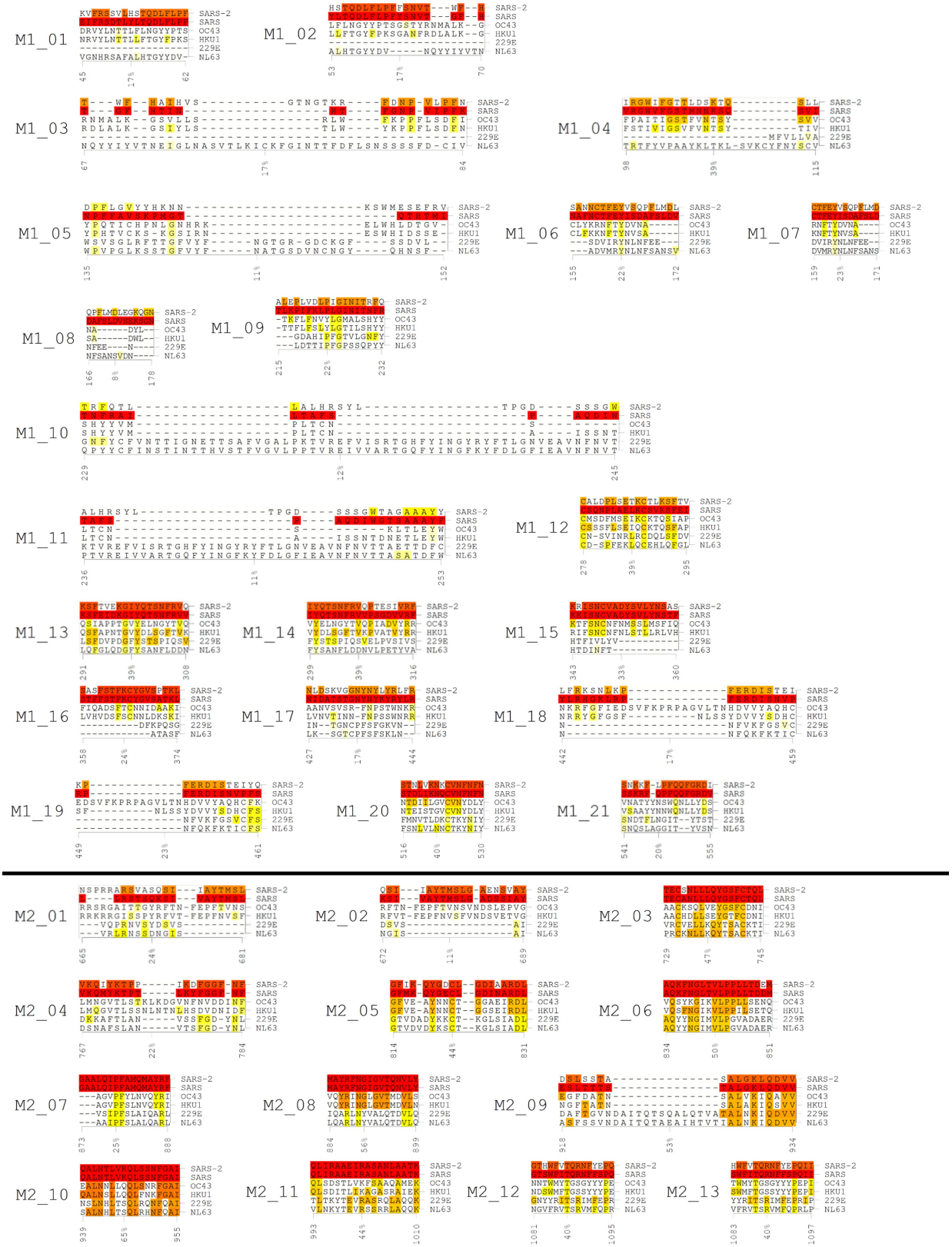

Extended Data Fig. 1 | Homology of reported MHC-II epitopes in the spike glycoprotein of SARS-CoV compared with SARS-CoV-2 and endemic hCoV strains. For each epitope, the respective section from a global sequence alignment between SARS-CoV, SARS-CoV-2 and the hCoVs NL63, 229E, HKU1 and OC43 is shown. Identical residues are colour-coded from white (no identity) to red (100% identity). Reported MHC-II epitopes are described further in Extended Data Table 1.

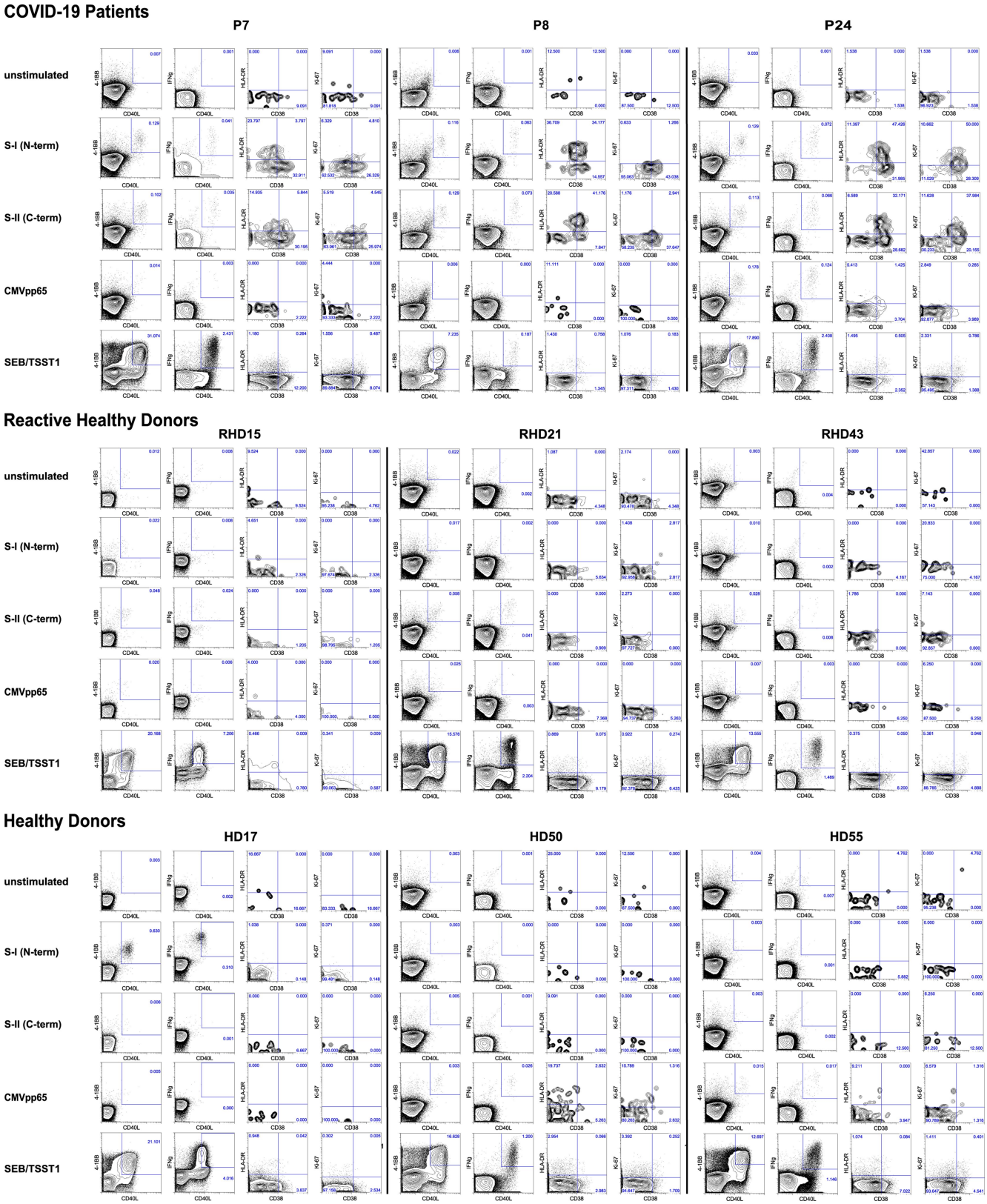

Extended Data Fig. 2 | Exemplary analyses gates and dot plots from patients with COVID-19, RHDs and HDs. FACS analysis was performed to determine the frequencies of S-I-reactive and S-II-reactive $CD4^+$ T cells and the ratios of $CD38^+$, $HLA\text{-}DR^+$ and $Ki\text{-}67^+$ cells among the S-I-reactive and S-II-reactive $CD4^+$ T cells.

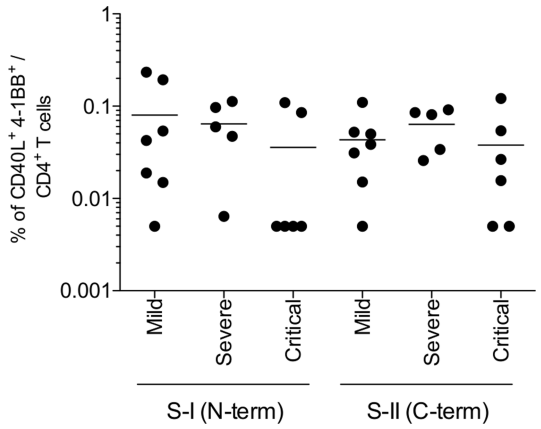

Extended Data Fig. 3 | Most S-I-non-reactive and S-II-non-reactive patients with COVID-19 had a critical disease stage. Frequencies of S-I- and S-II-reactive $CD4^+$ T cells in patients with COVID-19 are grouped according to disease severity for patients with mild ($n = 7$), severe ($n = 5$) or critical ($n = 6$) disease.

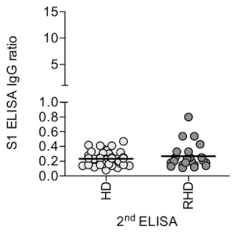

Extended Data Fig. 4 | Repeated serology of HDs confirms unexposed status of HDs and RHDs. SARS-CoV-2 S1 serology of HDs ($n = 43$) and RHDs ($n = 22$) more than 28 days after initial sampling. Anti-S1 IgG titres are expressed as a ratio normalized to the calibration well, which contained the provided control serum (as described in the manufacturing instructions).

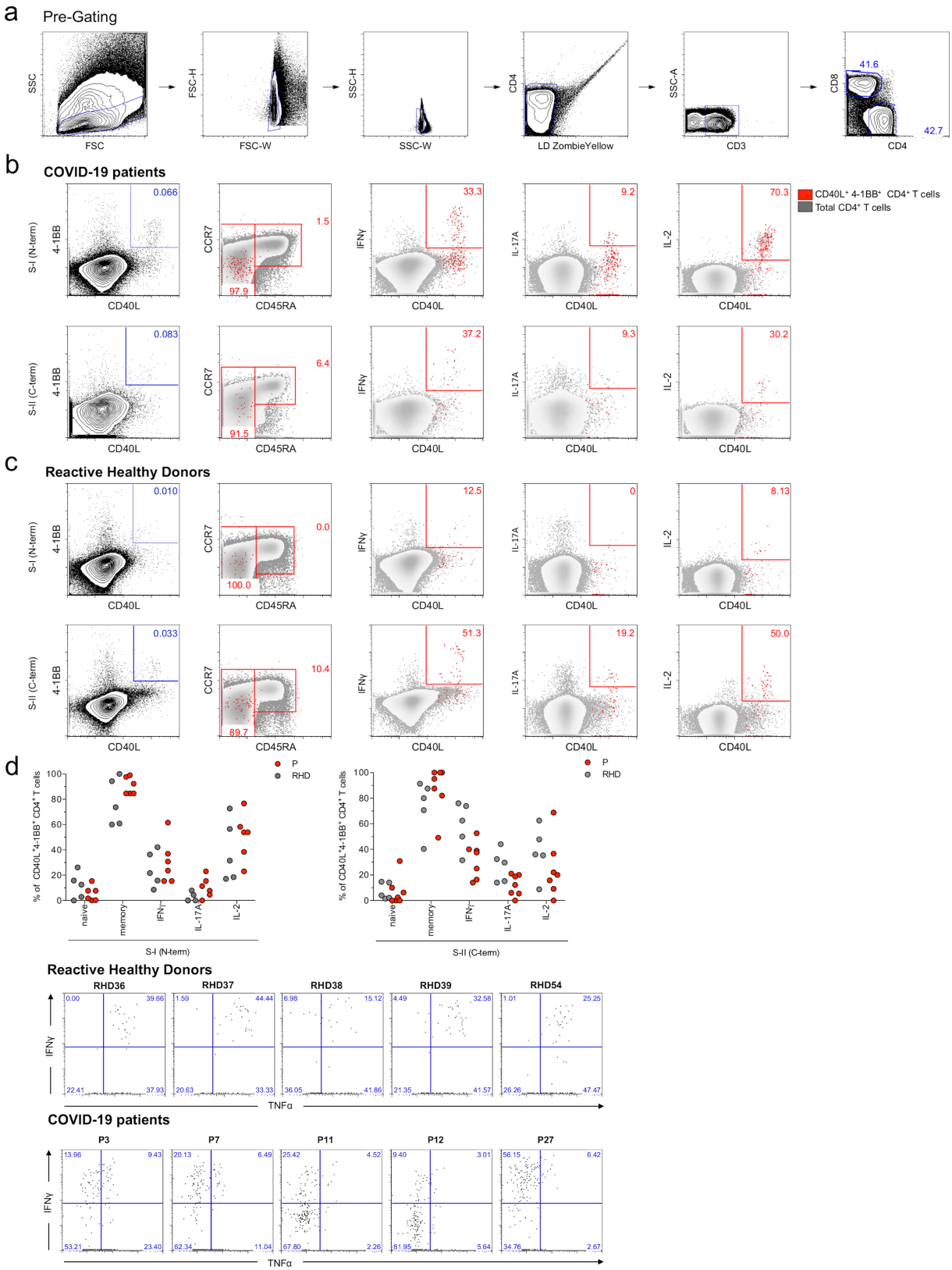

Extended Data Fig. 5 | Expression of cytokines and differentiation markers in S-I-reactive and S-II-reactive CD40L$^+$4-1BB$^+$CD4$^+$ T cells from patients with COVID-19 and RHDs. a, Gating schematic of one representative donor to select for CD3$^+$CD4$^+$ T cells and exclude dead cells and doublets. **b**, **c**, Determination of the differentiation marker and cytokine profiles of S-I- and S-II-reactive CD4$^+$ T cells shown for one patient with COVID-19 and one RHD after S-I and S-II peptide pool stimulation, respectively. SARS-CoV-2 S-reactive CD4$^+$ T cells were defined by CD40L and 4-1BB expression after stimulation and are displayed as red dots. Numbers are the frequencies of cytokine-expressing S-I/S-II-reactive CD4$^+$ T cells and the distribution of the naive (CCR7$^+$CD45RA$^+$) and memory (CCR7$^+$CD45RA$^-$ or CCR7$^-$CD45RA$^-$) phenotypes of S-I/S-II-reactive CD4$^+$ T cells, respectively. **d**, Diagrams summarizing the cytokine and differentiation marker distribution frequencies of S-I- and S-II-reactive CD4$^+$ T cells from patients with COVID-19 ($n = 7$) and RHDs ($n = 5$). **e**, Expression of TNF and IFNγ in S-II-reactive CD4$^+$ T cells from patients and RHDs. Five representative plots of TNF versus IFNγ expression in CD40L$^+$4-1BB$^+$CD4$^+$ T cells from RHDs and patients with COVID-19; gating strategy as shown in Fig. 2.

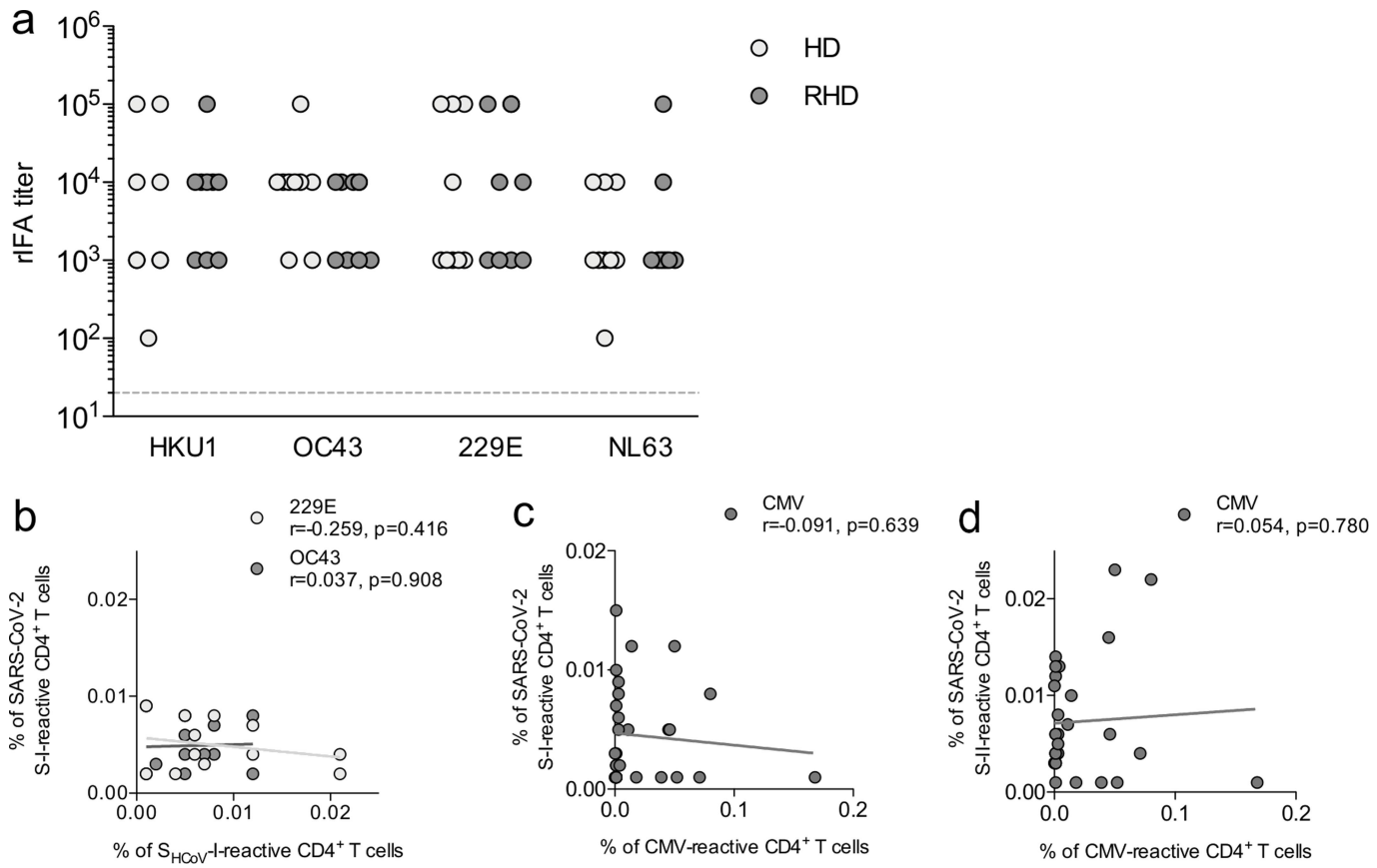

Extended Data Fig. 6 | hCoV-specific IgG antibody titres in HDs and RHDs and specificity of SARS-CoV-2-reactive T cells in HDs. a, IgG antibody titres against endemic coronavirus strains (hCoVs). VeroB4 cells expressing recombinant spike proteins of hCoV-HKU1, hCoV-OC43, hCoV-229E and hCoV-NL63 were used in a recombinant immunofluorescence assay (rIFA) as described previously[36]. Titres above 1:20 dilution were considered positive (indicated by the dashed line). HD, $n = 9$; RHD, $n = 9$. **b**–**d**, Frequencies of SARS-CoV-2 S-I-reactive CD4$^+$ T cells in HDs do not correlate with frequencies of S_{hCoV}-I-reactive or CMV-reactive CD4$^+$ T cells. Frequencies of SARS-CoV-2 S-II-reactive CD4$^+$ T cells in HDs do not correlate with frequencies of CMV-reactive CD4$^+$ T cells. **b**, Scatter plot of S_{hCoV}-I-reactive CD4$^+$ T cell frequencies (229E, $n = 12$; OC43, $n = 9$) and SARS-CoV-2 S-I-reactive CD4$^+$ T cell frequencies. **c**, Scatter plot of SARS-CoV-2 S-I-reactive CD4$^+$ T cell and CMV-reactive CD4$^+$ T cell frequencies ($n = 21$). **d**, Scatter plot of SARS-CoV-2 S-II-reactive CD4$^+$ T cell and CMV-reactive CD4$^+$ T cell frequencies ($n = 21$). **b**–**d**, Correlation coefficients (r) were calculated by Pearson correlation and the related P values are based on t-distributions.

Extended Data Table 1 | Reported MHC-II epitopes in the spike glycoprotein of SARS-CoV

ID	PepMix™	Sequence	Maximum identity common cold viruses (%)	Identity SARS-CoV-2	Start position SARS	Stop position SARS	Reference
M1_1	1	EIFRSDTLYLTQDLFLPF	16,7	66,7	45	62	14
M1_2	1	YLTQDLFLPFYSNVTGFH	16,7	77,8	53	70	14
M1_3	1	TGFHTINHTFGNPVIPFK	16,7	55,6	67	84	14
M1_4	1	VRGWVFGSTMNNKSQSVI	38,9	50	98	115	14
M1_5	1	NPFFAVSKPMGTQTHTMI	11,1	16,7	135	152	14
M1_6	1	NAFNCTFEYISDAFSLDV	22,2	55,6	155	172	14
M1_7	1	CTFEYISDAFSLD	23,1	61,5	159	171	14
M1_8	1	DAFSLDVSEKSGN	7,7	38,5	166	178	14
M1_9	1	TLKPIFKLPLGINITNFR	22,2	55,6	215	232	14
M1_10	1	TNFRAILTAFSPAQDIW	11,8	23,5	229	245	14
M1_11	1	TAFSPAQDIWGTSAAAYF	11,1	27,8	236	253	14
M1_12	1	CSQNPLAELKCSVKSFEI	38,9	50	278	295	14
M1_13	1	KSFEIDKGIYQTSNFRVV	38,9	77,8	291	308	14
M1_14	1	IYQTSNFRVVPSGDVVRF	38,9	72,2	299	316	14
M1_15	1	KKISNCVADYSVLYNSTF	33,3	83,3	343	360	14
M1_16	1	STFFSTFKCYGVSATKL	23,5	82,4	358	374	13;14
M1_17	1	NIDATSTGNYNYKYRYLR	16,7	55,6	427	444	13
M1_18	1	YLRHGKLRPFERDISNVP	16,7	50	442	459	14
M1_19	1	RPFERDISNVPFS	23,1	53,8	449	461	14
M1_20	1	STDLIKNQCVNFNFN	40	80	516	530	15
M1_21	1	SSKRFQPFQQFGRDV	20	73,3	541	555	15
		Mean Identity PepMix™ 1	23,2	57,5			
M2_1	2	LLRSTSQKSIVAYTMSL	23,5	58,8	665	681	14
M2_2	2	KSIVAYTMSLGADSSIAY	11,1	72,2	672	689	14
M2_3	2	TECANLLLQYGSFCTQL	47,1	94,1	729	745	13
M2_4	2	VKQMYKTPTLKYFGGFNF	22,2	77,8	767	784	14
M2_5	2	GFMKQYGECLGDINARDL	44,4	83,3	814	831	14
M2_6	2	AQKFNGLTVLPPLLTDDM	50	94,4	834	851	14
M2_7	2	GAALQIPFAMQMAYRF	25	100	873	888	14
M2_8	2	MAYRFNGIGVTQNVLY	56,2	100	884	899	14
M2_9	2	ESLTTTSTALGKLQDVV	52,9	70,6	918	934	14
M2_10	2	QALNTLVKQLSSNFGAI	64,7	100	939	955	14
M2_11	2	QLIRAAEIRASANLAATK	44,4	100	993	1010	14
M2_12	2	GTSWFITQRNFFSPQ	40	73,3	1081	1095	15
M2_13	2	SWFITQRNFFSPQII	40	73,3	1083	1097	14
		Mean Identity PepMix™ 2	40,1	84,4			

MHC-II epitopes of the spike protein of SARS-CoV are shown with maximum identity calculations for SARS-CoV-2 and the hCoVs NL63, 229E, HKU1 and OC43.

Extended Data Table 2 | Baseline characteristics of hospitalized patients with COVID-19

COVID-19 patients						
ID	**Severity**	**Gender**	**Age**	**Chief complaints at admission**	**ICU (y/n)**	**Sampling (day)***
P01	mild	m	21	Fever, dry cough, malaise	n	39
P03	mild	m	45	Fever, dry cough, runny nose	n	25
P10	mild	f	50	Fever, dry cough, myalgia, cephalgia, diarrhea	n	17
P18	mild	f	60	Fever, myalgia, cephalgia, runny nose	n	21
P19	mild	m	52	Dry cough, cephalgia, arthralgia, nausea	n	11
P23	mild	f	44	Fever	n	5
P27	mild	f	41	Fever, dry cough	n	13
P06	severe	m	24	Fever, dyspnea, malaise	y	11
P07	severe	m	33	Fever, dry cough, dyspnea, myalgia	n	5
P11	severe	m	61	Fever, dry cough, dyspnea, sore throat	y	12
P16	severe	m	74	Fever, dry cough, dyspnea, malaise	y	12
P24	severe	m	64	Fever, dry cough, dyspnea	y	19
P08	critical	m	63	Fever, dyspnea	y	2
P12	critical	m	75	Fever, dyspnea, malaise	y	8
P14	critical	m	81	Fever, dyspnea	y	8
P15	critical	m	54	Dry cough, dyspnea	y	6
P20	critical	f	53	Dry cough, dyspnea	y	11
P21	critical	m	52	Dry cough, dyspnea	y	9

f, female; m, male; n, no; y, yes.
*Days after onset of symptoms.

Extended Data Table 3 | Baseline characteristics of healthy donors

Healthy donors							
ID	**Gender**	**Age**	**Health status**	**ID**	**Gender**	**Age**	**Health status**
HD01	m	56		HD38	f	30	Allergies
HD02	m	48		HD39	f	41	
HD03	m	37		HD40	f	53	
HD04	f	40		HD41	m	42	
HD05	f	22		HD42	f	55	
HD06	m	30		HD43	m	25	
HD07	m	25		HD44	f	53	Hashimoto Thyreoiditis
HD08	m	41		HD45	f	47	
HD09	m	37		HD46	f	31	
HD10	m	40		HD47	f	46	
HD11	f	28		HD48	m	31	
HD12	f	43		HD49	m	44	
HD13	m	44	Allergies	HD50	f	60	
HD14	f	27		HD51	f	43	
HD15	m	32		HD52	f	20	
HD16	m	24		HD53	f	46	
HD17	m	42		HD54	m	24	
HD18	m	40		HD55	f	40	
HD19	f	26		HD56	f	40	
HD20	f	33		HD57	f	50	
HD21	m	30		HD58	f	30	
HD22	m	29		HD59	f	46	Allergies
HD23	f	38		HD60	f	31	
HD24	m	25		HD61	f	52	
HD25	m	48		HD62	f	53	Adenoma (surgically removed)
HD26	f	30		HD63	f	40	
HD27	m	64		HD64	f	27	
HD28	f	22		HD65	m	52	
HD29	f	40		HD66	f	42	
HD30	f	30		HD67	f	25	
HD34	f	55		HD68	m	38	
HD35	m	38	Thyroid dysfunction	HD70	f	22	
HD36	m	27		HD71	m	30	
HD37	f	26		HD72	f	64	

Extended Data Table 4 | Baseline characteristics of seven additional patients with COVID-19

ID	Severity	Gender	Age	Chief complaints at admission	ICU (y/n)	Sampling (day)*
P153	mild	m	56	Dry cough, dyspnea, aeguisa	n	11
P158	mild	m	26	Fever, dry cough	n	10
P51	severe	m	79	Fever, dry cough, dyspnea	y	52
P131	severe	f	71	Malaise, rash	y	33
P157	severe	m	50	Fever, cough, malaise	y	23
P134	critical	m	27	Dyspnea	y	39
P142	critical	m	62	Fever cough, dyspnea	y	53

Seven patients with COVID-19 were enrolled for the analysis of cytokine expression; cytokines were stained with antibodies and expression levels were analysed using flow cytometry.
*Days after onset of symptoms.

nature research

Corresponding author(s): Andreas Thiel

Last updated by author(s): Sep 9, 2020

Reporting Summary

Nature Research wishes to improve the reproducibility of the work that we publish. This form provides structure for consistency and transparency in reporting. For further information on Nature Research policies, see Authors & Referees and the Editorial Policy Checklist.

Statistics

For all statistical analyses, confirm that the following items are present in the figure legend, table legend, main text, or Methods section.

n/a	Confirmed
☐	☒ The exact sample size (*n*) for each experimental group/condition, given as a discrete number and unit of measurement
☐	☒ A statement on whether measurements were taken from distinct samples or whether the same sample was measured repeatedly
☐	☒ The statistical test(s) used AND whether they are one- or two-sided *Only common tests should be described solely by name; describe more complex techniques in the Methods section.*
☒	☐ A description of all covariates tested
☐	☒ A description of any assumptions or corrections, such as tests of normality and adjustment for multiple comparisons
☐	☒ A full description of the statistical parameters including central tendency (e.g. means) or other basic estimates (e.g. regression coefficient) AND variation (e.g. standard deviation) or associated estimates of uncertainty (e.g. confidence intervals)
☒	☐ For null hypothesis testing, the test statistic (e.g. *F*, *t*, *r*) with confidence intervals, effect sizes, degrees of freedom and *P* value noted *Give P values as exact values whenever suitable.*
☒	☐ For Bayesian analysis, information on the choice of priors and Markov chain Monte Carlo settings
☒	☐ For hierarchical and complex designs, identification of the appropriate level for tests and full reporting of outcomes
☐	☒ Estimates of effect sizes (e.g. Cohen's *d*, Pearson's *r*), indicating how they were calculated

Our web collection on statistics for biologists contains articles on many of the points above.

Software and code

Policy information about availability of computer code

Data collection	Miltenyi MACSquantify software v2.13 was used for flow cytometry data collection.
Data analysis	All the softwares and there version information are shown her. FlowJo (v9.9.6) was used for all FACS analyses. Microsoft Excel (v.14.1.0) was used to collect and arrange data and patient / donor information. GraphPad Prism (v5.0b and v8.4.2. (464)) was used to analyze data and create plots. Sequence alignments have been performed using R (v3.6.1) including package ClustalX (Larkin,M.A., Blackshields, G., Brown, N.P., Chenna, R., McGettigan, P.A., McWilliam, H., Valentin, F., Wallace, I.M., Wilm, A., Lopez, R., Thompson, J.D., Gibson, T.J., Higgins, D.G. (2007) Clustal W and Clustal X version 2.0. Bioinformatics, 23:2947-2948.) and using the Needlemann-Wunsch algorithm.

For manuscripts utilizing custom algorithms or software that are central to the research but not yet described in published literature, software must be made available to editors/reviewers. We strongly encourage code deposition in a community repository (e.g. GitHub). See the Nature Research guidelines for submitting code & software for further information.

Data

Policy information about availability of data

All manuscripts must include a data availability statement. This statement should provide the following information, where applicable:

- Accession codes, unique identifiers, or web links for publicly available datasets
- A list of figures that have associated raw data
- A description of any restrictions on data availability

All flow cytometry data are made available in the FlowRepository,org (experiment ID: FR-FCM-Z2K3). An additional Supplementary Figure displaying the individual gating strategy for all donors is available in the online version of the paper.

Field-specific reporting

Please select the one below that is the best fit for your research. If you are not sure, read the appropriate sections before making your selection.

☒ Life sciences ☐ Behavioural & social sciences ☐ Ecological, evolutionary & environmental sciences

For a reference copy of the document with all sections, see nature.com/documents/nr-reporting-summary-flat.pdf

Life sciences study design

All studies must disclose on these points even when the disclosure is negative.

Sample size	No sample size calculation was performed. Within COVID-19 patients, 83% exhibited T cell reactivity to the Spike glycoprotein of SARS-CoV2. Within the healthy donors recruited, 35% were identified as reactive healthy donors. With the proportions, the recruited numbers of subjects are sufficient.
Data exclusions	No data were excluded from the analysis.
Replication	We remeasured several donors (accompanied by anti-SARS-CoV-2 IgG antibody testing) at later timepoints and used another Spike glycoprotein peptide pool from Miltenyi to ensure reproducibility of T cell reactivity in SARS-CoV-2 naive donors.
Randomization	No randomization was performed since it was not applicable to the study.
Blinding	Blinding was not applicable to this study.

Reporting for specific materials, systems and methods

We require information from authors about some types of materials, experimental systems and methods used in many studies. Here, indicate whether each material, system or method listed is relevant to your study. If you are not sure if a list item applies to your research, read the appropriate section before selecting a response.

Materials & experimental systems

n/a	Involved in the study
☐	☒ Antibodies
☒	☐ Eukaryotic cell lines
☒	☐ Palaeontology
☒	☐ Animals and other organisms
☐	☒ Human research participants
☒	☐ Clinical data

Methods

n/a	Involved in the study
☒	☐ ChIP-seq
☐	☒ Flow cytometry
☒	☐ MRI-based neuroimaging

Antibodies

Antibodies used	CD69-APCCy7 BioLegend Cat# 310914, RRID:AB_314849 CD4-BV605 BioLegend Cat# 300556, RRID:AB_2564391 CD8-PerCp BioLegend Cat# 344708, RRID:AB_1967149 IFNg-AlexaFluor700 BioLegend Cat# 502520, RRID:AB_528921 TNFa-PB BioLegend Cat# 502920, RRID:AB_528965 CD38-PeVio770 Miltenyi Biotec Cat# 130-118-982, RRID:AB_2751601 HLADR-VG Miltenyi Biotec Cat# 130-111-795, RRID:AB_2652164 CD154-APC Miltenyi Biotec Cat# 130-113-603, RRID:AB_2726191 CD137-PE BD Biosciences Cat# 555956, RRID:AB_396252 CD154-BV421 BioLegend Cat# 310824, RRID:AB_2562721 IL-2-APC BD Biosciences Cat# 341116, RRID:AB_400574 IL-17A-APCCy7 BioLegend Cat# 512320, RRID:AB_10613103 CCR7-AlexaFluor488 BioLegend Cat# 353206, RRID:AB_10916389 CD45RA-PeCy7 BioLegend Cat# 304126, RRID:AB_10708879 CD3-V500 BD Biosciences Cat# 560770, RRID:AB_1937322
Validation	All antibodies are established, well described and published elsewhere. Informations are accessible on the manufacturers websites under Catalogue or RRID numbers.

Human research participants

Policy information about studies involving human research participants

Population characteristics	The study included: - 18 COVID-19 patients (Table 1):age mean 52.6, range: 21-81 yrs; gender: female ratio 27.8%; sampling day (post symptom onset): mean 14.9, range: 2-39 - 7 additional COVID-19 patients (Extended data Table 3): age mean 53, range: 10-79 yrs; gender: female ratio 14.3%; sampling day (post symptom onset): mean 31.6, range: 10-53 - 68 healthy donors (age mean 41.93, range: 20-64 yrs; gender: female ratio 59%) All healthy donors stated to be free of symptoms indicating an acute infection.
Recruitment	Patients were hospitalised in the Charité. The patients were selected based on the disease severiyt to achieve a balanced representation of the three disease serverity groups.
Ethics oversight	Institutional Review Board of the Charité.

Note that full information on the approval of the study protocol must also be provided in the manuscript.

Flow Cytometry

Plots

Confirm that:

☐ The axis labels state the marker and fluorochrome used (e.g. CD4-FITC).

☐ The axis scales are clearly visible. Include numbers along axes only for bottom left plot of group (a 'group' is an analysis of identical markers).

☒ All plots are contour plots with outliers or pseudocolor plots.

☒ A numerical value for number of cells or percentage (with statistics) is provided.

Methodology

Sample preparation	Peripheral blood mononuclear cells (PBMC) were isolated from heparinized whole blood by gradient density centrifugation according to manufacturer's instructions (Leucosep tubes, Greiner; Biocoll, Bio&SELL). Stimulation was conducted with 5x10e6 PBMC in RPMI 1640 medium (Gibco) supplemented with 10% heat inactivated AB serum (Pan Biotech), 100 U/ml penicillin (Biochrom), 0.1 mg/ml streptomycin (Biochrom), and PepMixTM SARS-CoV-2 in the presence of 1 µg/ml purified anti-CD28 (clone CD28.2, BD Biosciences). PepMixTM SARS-CoV-2 (Spike Glycoprotein) subpool 1 covering the N-terminal aa 1-643 (abbreviated to "S-I (N-term)") containing 158 15-mers overlapping by 11 and PepMixTM SARS-CoV-2 (Spike Glycoprotein) subpool 2 covering the C-terminal aa 633-1273 (abbreviated to "S-II (C-term)") (JPT) containing 156 15-mers overlapping by 11 and one 17-mer at C-terminus were used at 1 µg/ml per peptide, respectively. Stimulation controls were performed with equal concentrations of DMSO in PBS (unstimulated) or 1.5 mg SEB/1.0 mg TSST1 (Sigma-Aldrich) and PepMixTM CMV pp65 (Miltenyi) as positive controls, respectively. Incubation was performed at 37˚C, 5% CO2 for 14h with 10 µg/ml brefeldin A (Sigma- Aldrich) added after 2 h. Stimulation was stopped by incubation in 20 mM EDTA for 5 min and surface staining conducted for 15 min with the following fluorochrome conjugated antibodies titrated to their optimal concentrations: CD38-PE-Vio770 (clone REA671, Miltenyi), CD69-APC-Cy7 (FN50, Biolegend), HLAD-DR-VioGreen (REA805, Miltenyi), CD4-BrilliantViolet605 (RPA-T4, Biolegend), CD8-PerCP (SK1, Biolegend) with 1 mg/ml Beriglobin (CSL Behring) added prior to the staining. For exclusion of dead cells, Zombie Yellow fixable viability staining (Biolegend) was added for the last 10 min of incubation. Fixation and permeabilization were performed with eBioscienceTM FoxP3 fixation and PermBuffer (Invitrogen) according to the manufacturer's protocol and intracellular staining carried out for 30 min in the dark at room temperature with Beriglobin added prior to intracellular staining with 4-1BB-PE (clone 4B4-1, BD), CD40L-APC (5C8, Miltenyi) and Ki-67-AlexaFluor488 (B56, BD). For intracellular cytokine staining, we employed different antibodies. Surface staining was performed with CD3-V500 (SP34-2, BD), CD8-PerCP (SK1, Biolegend), CD4-BrilliantViolet605 (RPA-T4, Biolegend), CCR7-AlexaFluor488 (G043H7, Biolegend), CD45RA-PE-Cy7 (HI100, Biolegend). IFN-γ-AlexaFluor700, CD40L-BrilliantViolet421 (24-31, Biolegend), IL-2-APC (5344.111, BD), 4-1BB-PE (4B4-1, BD) and IL-17A-APC-Cy7 (BL168, Biolegend) were utilized for intracellular staining after fixation and permeabilization using BD FACSLysing Buffer and BD Perm2 Buffer, according to manufacturer's instructions.
Instrument	Samples were measured on a MACSQuant® Analyzer 16 and the instrument performance monitored daily with Rainbow Calibration Particles (BD).
Software	Miltenyi MACSquantif software (v2.13) and FlowJo (v9.9.6)
Cell population abundance	Cells have not been enriched or sorted, except by the generation of SARS-CoV-2-S-II reactive CD4 T cell lines. Data are shown within ex vivo stimulated peripheral blood mononuclear cells.
Gating strategy	All recorded events were gated according to FSC and SSC as lymphocytes; single cells were further selected using FSC-H vs. FSC-W and again using SSC-H vs. SSC-W. Subsequently living cells were identified as ZombieYellow negative cells gated against CD4-BV605. An artefact population in some samples (probably induced by DMSO) was observed disturbing data analysis and was gated out using V500 vs V450. The subsequent gating scheme is depicted in Fig.2a and Fig. 3a.

☒ Tick this box to confirm that a figure exemplifying the gating strategy is provided in the Supplementary Information.